Polyethylenimine Crosslinked 3-Aminopropyltriethoxysilane Grafted Multiwall Carbon Nanotubes for Efficient Adsorption of Reactive Yellow 2 from Water

Zhuo Wang and Sung Wook Won *

Posted Date: 9 January 2023

doi: 10.20944/preprints202301.0154.v1

Keywords: Amine functionalized MWCNTs; Reactive yellow 2; Adsorption; Rapid removal; Ionic strength; Reusability

Article

Polyethylenimine Crosslinked 3-Aminopropyltriethoxysilane Grafted Multiwall Carbon Nanotubes for Efficient Adsorption of Reactive Yellow 2 from Water

Zhuo Wang [1] and Sung Wook Won [1,2,*]

[1] Department of Ocean System Engineering, Gyeongsang National University, 2 Tongyeonghaean-ro, Tongyeong, Gyeongnam 53064, Republic of Korea; wz928661411@gnu.ac.kr
[2] Department of Marine Environmental Engineering, Gyeongsang National University, 2 Tongyeonghaean-ro, Tongyeong, Gyeongnam 53064, Republic of Korea
* Correspondence: sungukw@gnu.ac.kr; Tel.: +82 55 772 9136

Abstract: This research intended to report amine-functionalized multiwall carbon nanotubes (MWCNTs) prepared by a simple method for efficient and rapid removal of Reactive Yellow 2 (RY2) from water. EDS analysis showed that the N content increased from 0 to 2.42% and from 2.42 to 8.66% after modification by APTES and PEI, respectively. BET analysis displayed that the specific surface area, average pore size, and total pore volume were reduced from 405.22 to 176.16 m^2/g, 39.67 to 6.30 nm, and 4.02 to 0.28 cm^3/g, respectively. These results proved that the PEI/APTES-MWCNTs were successfully prepared. pH edge experiment indicated that pH 2 was optimal for RY2 removal. At pH 2 and 25 °C, the time required for adsorption equilibrium was 10, 15, and 180 min at initial concentrations of 50, 100, and 200 mg/L, respectively; and the maximum RY2 uptake calculated by the Langmuir model was 714.29 mg/g. Thermodynamic studies revealed that the adsorption process was spontaneous and endothermic. 0-0.1 mol/L of NaCl showed negligible effect on RY2 removal by PEI/APTES-MWCNTs. Five adsorption/desorption cycles confirmed the good reusability of PEI/APTES-MWCNTs in RY2 removal. Overall, the PEI/APTES-MWCNTs are a potential and efficient adsorbent for reactive dye wastewater treatment.

Keywords: amine functionalized MWCNTs; reactive yellow 2; adsorption; rapid removal; ionic strength; reusability

1. Introduction

The 2018 edition of the United Nations World Water Development Report indicated that around 4 billion people worldwide face short- or long-term water scarcity; by 2050, this population will grow to approximately 6 billion, which may even be underestimated [1]. Water scarcity can lead to various social and environmental problems and, ultimately, to war [2,3]. The textile industry is one of the industries that exacerbate water scarcity. On the one hand, the textile industry is water-consuming, and on the other hand, its wastewater discharge is enormous. The immediate release of untreated textile wastewater can cause severe pollution of water sources [4]. Reactive dyes are among the most widely used dyes in the textile industry. The typical characteristics of their wastewater include difficult biodegradation, high coloration even at low concentrations, and high organic concentrations [5]. Reactive dyes and their degradation byproducts are toxic, carcinogenic, teratogenic, and mutagenic [6]. Adsorption is considered one of the most desirable methods for dye removal due to its low cost, simplicity of operation, low energy requirements, and recoverable adsorbent [7].

In recent decades, nanomaterials have attracted much attention due to their particular structures and unique physicochemical properties. Nanomaterials, including metal oxides, carbon nanotubes,

Preprints (www.preprints.org) | NOT PEER-REVIEWED | Posted: 9 January 2023 doi:10.20944/preprints202301.0154.v1

graphene nanosheets, silicon nanospheres, and polymeric nanofibers, have been used as adsorbents to reduce various pollutants from wastewater [8,9]. Among them, multiwall carbon nanotubes (MWCNTs) are considered excellent adsorbents for the removing organic dyes from water because of their large specific surface area, easy surface modification, and good chemical stability [10,11]. Since the adsorption capacity of pristine MWCNTs for organic dyes was relatively low, many researchers have used surface modification methods, such as amine-functionalization methods, to improve their adsorption capacity [11]. However, the preparation of amine-functionalized MWCNTs often involves the utilization of toxic organic solvents, extreme conditions, and complex procedures [12–15]. Therefore, it is still of great significance to explore more accessible and greener ways to prepare amine-functionalized MWCNTs.

In this study, amine-functionalized MWCNTs, polyethylenimine (PEI) crosslinked 3-Aminopropyltriethoxysilane (APTES) grafted MWCNTs (PEI/APTES-MWCNTs), was prepared in a more straightforward and organic solvent-free approach. Since, the adsorption of reactive dyes by amine-functionalized MWCNTs has rarely been reported. Reactive Yellow 2 (RY2), a widely used reactive dye was selected as a representative to evaluate the adsorption performance of reactive dyes on PEI/APTES-MWCNTs. The effect of pH, contact time, initial concentration, temperature, and ionic strength were estimated to understand the adsorption performance of PEI/APTES-MWCNTs towards RY2. The reusability of the adsorbent was also investigated.

2. Results and Discussion

In this work, PEI/APTES-MWCNTs were prepared by a simple and feasible method. The one-point-check experiment was performed to verify the successful preparation of PEI/APTES-MWCNTs. As shown in Figure 1, the adsorption capacity of MWCNTs was increased 1.3 times after grafting APTES on their surface. After crosslinking with PEI, the adsorption capacity increased to about 2.8 times that of the pristine MWCNTs. This result proved that the PEI/APTES-MWCNTs were successfully prepared. FE-SEM-EDS and BET analyses were performed to investigate the prepared adsorbents further.

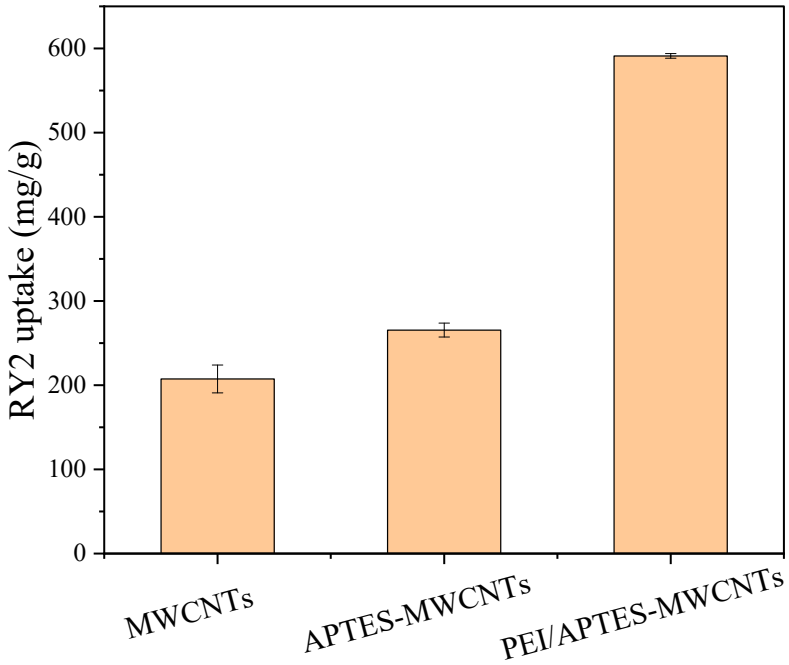

Figure 1. RY2 uptake on MWCNTs, APTES-MWCNTs, and PEI/APTES-MWCNTs. (C_i = 200 mg/L, sorbent amount = 10 mg, pH = 2).

Preprints (www.preprints.org) | NOT PEER-REVIEWED | Posted: 9 January 2023 doi:10.20944/preprints202301.0154.v1

2.1. FE-SEM-EDS Analysis

The surface morphology of the materials was observed using a field-emission scanning electron microscope (FE-SEM) and their corresponding elemental mappings were recorded using an energy-dispersive spectrometer (EDS). As shown in Figure 2a,c, the spacing between the APTES-grafted MWCNTs was lower than that of the original MWCNTs. In addition, numerous MWCNTs aggregated into bundles, as shown in the red circles in Figure 2c. The interval between MWCNTs after PEI crosslinking was smaller and more MWCNTs were entangled, as shown in the red circle (Figure 2e). This higher entangled structure may be due to the functionalization of MWCNTs [14]. The aggregation structure may be due to the enhanced interactions between functionalized MWCNTs. The PEI/APTES-MWCNTs show severe entanglement compared to the pristine MWCNTs and APTES-MWCNTs. The reason was that the PEI molecules crosslinked the MWCNTs that were originally present in a dispersed state. The FE-SEM images may confirm that APTES and PEI successfully modified the MWCNTs. To further verify this conclusion, the EDS analysis was conducted. Figure 2b revealed that the MWCNTs did not contain N and Si elements. As demonstrated in Figure 2d, N and Si elements appeared in the map sum spectrum of APTES-MWCNTs, indicating that APTES was grafted on MWCNTs surface. With further modification with PEI, the N elemental content was greatly increased (Figure 2f), and the atomic percentage of N in PEI/APTES-MWCNTs was approximately 3.6 times higher than in APTES-MWCNTs. Overall, FE-SEM-EDS analysis proved that APTES and PEI successfully modified MWCNTs.

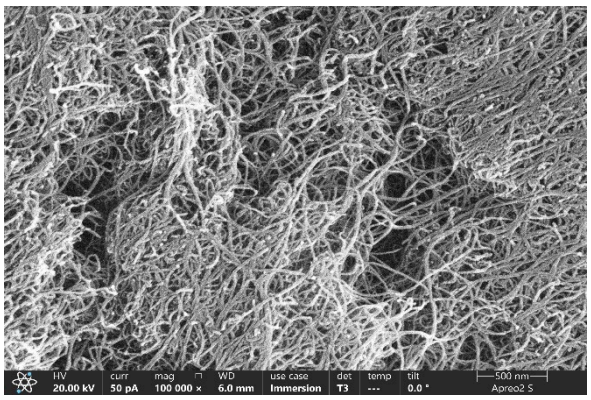

(**a**)

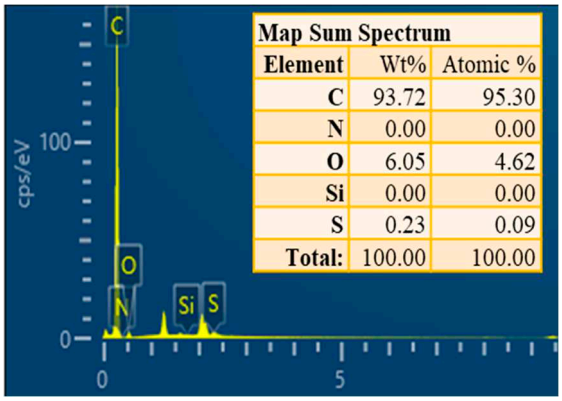

Map Sum Spectrum		
Element	Wt%	Atomic %
C	93.72	95.30
N	0.00	0.00
O	6.05	4.62
Si	0.00	0.00
S	0.23	0.09
Total:	100.00	100.00

(**b**)

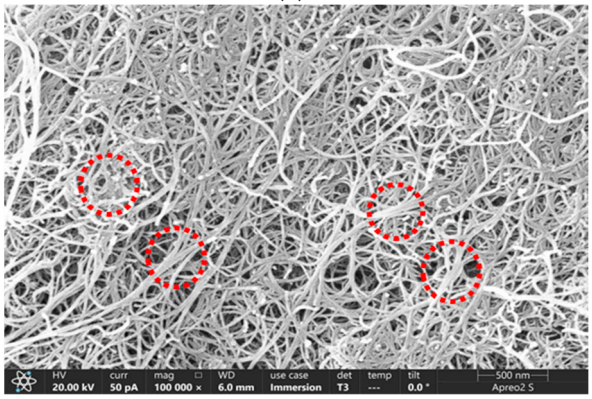

(**c**)

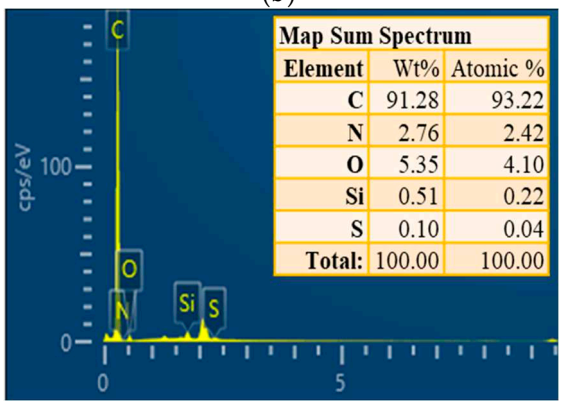

Map Sum Spectrum		
Element	Wt%	Atomic %
C	91.28	93.22
N	2.76	2.42
O	5.35	4.10
Si	0.51	0.22
S	0.10	0.04
Total:	100.00	100.00

(**d**)

Preprints (www.preprints.org) | NOT PEER-REVIEWED | Posted: 9 January 2023 doi:10.20944/preprints202301.0154.v1

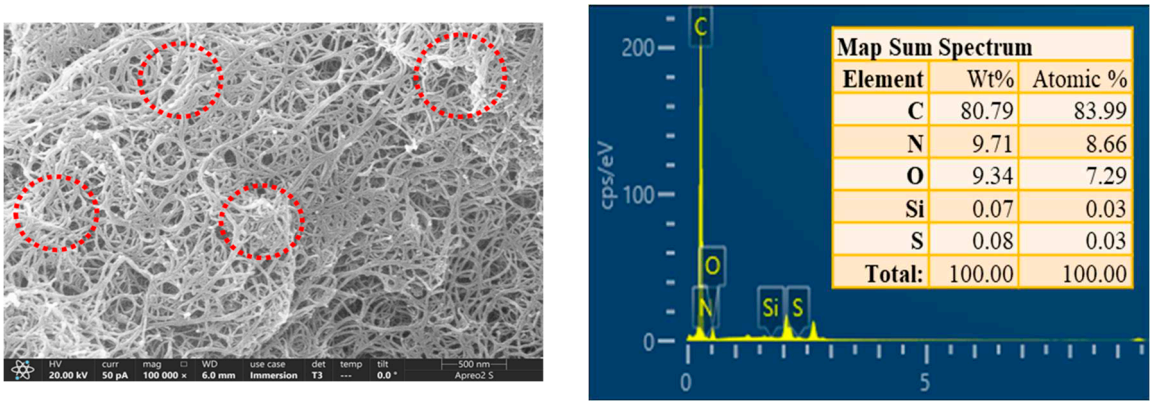

(**e**) (**f**)

Figure 2. FE-SEM image and map sum spectrum of (a, b) MWCNTs, (c, d) APTES-MWCNTs, and (e, f) PEI/APTES-MWCNTs.

2.2. BET Analysis

The specific surface area, average pore size, and total pore volume of MWCNTs, APTES-MWCNTs, and PEI/APTES-MWCNTs were measured by N_2 adsorption-desorption experiments, the results are present in Figure 3 and Table 1, respectively. According to the IUPAC classification [16], the curve of MWCNTs is type IV isotherm with a type H1 hysteresis loop, while the curves of APTES-MWCNTs and PEI/APTES-MWCNTs are type IV isotherm with type H3 hysteresis loop (Figure 3a). These results indicate the presence of mesopores [17,18]. The pore size distributions of the samples are shown in Figure 3b. It can be seen that MWCNTs have large pore volumes, with many of their pore size exceeding 15 nm (the diameter of the commercial MWCNTs are 8-15 nm); this should be associated with the secondary apertures created by the aggregation of MWCNTs [19]. The pore volumes and the number of large pores (> 15 nm) of MWCNTs were significantly reduced due to the modification by APTES and PEI. These results were probably attributed to APTES and PEI blocking of the pores and interspace regions between MWCNTs. As a result, the specific surface area, average pore size, and total pore volume of APTES-MWCNTs and PEI/APTES-MWCNTs were much smaller than those of the MWCNTs (Table 1). Although the specific surface area and total pore volume of PEI/APTES-MWCNTs were much smaller than those of MWCNTs, their ability to adsorb RY2 was greatly enhanced (Figure 1). The reduction of specific surface area and total pore volume was attributed to the large number of adsorption sites provided by the amine groups of PEI, indicating that PEI was successfully crosslinked to the surface of APTES-MWCNTs.

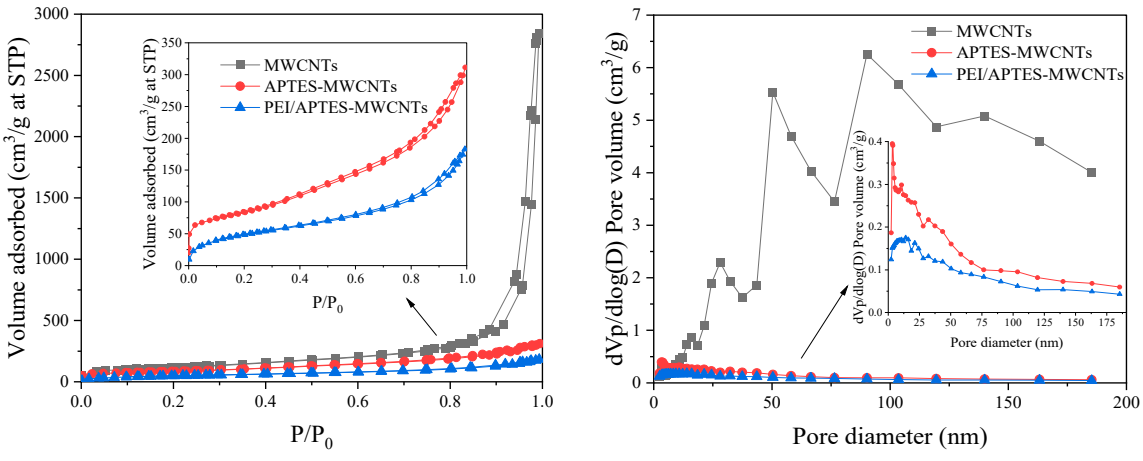

(**a**) (**b**)

Figure 3. (a) N_2 adsorption-desorption isotherms and (b) pore size distribution of MWCNTs, APTES-MWCNTs, and PEI/APTES-MWCNTs.

Preprints (www.preprints.org) | NOT PEER-REVIEWED | Posted: 9 January 2023 doi:10.20944/preprints202301.0154.v1

Table 1. Specific surface area, average pore size, and total pore volume of the materials.

Sample	Specific Surface Area (m^2/g)	Average Pore Size (nm)	Total Pore Volume (cm^3/g)
MWCNTs	405.22	39.67	4.02
APTES-MWCNTs	289.65	6.50	0.47
PEI/APTES-MWCNTs	176.16	6.30	0.28

2.3. Effect of pH

Solution pH is an important factor affecting the adsorption performance of adsorbents. The relationship between the solution pH and the adsorption capacity of RY2 on PEI/APTES-MWCNTs was investigated by altering the initial pH of the RY2 solution under controlled experimental conditions (Figure 4a). The PEI/APTES-MWCNTs showed the highest adsorption capacity (593.6 ± 1.3 mg/g) for RY2 at pH 2.0. The dye uptake on PEI/APTES-MWCNTs slightly decreased to 586.4 ± 3.8 mg/g with increasing pH to 4.0. Hereafter, the adsorption capacity of PEI/APTES-MWCNTs for RY2 dropped sharply to 224.0 ± 8.3 mg/g when the pH was raised to 12.0. To further explain the adsorption performance of PEI/APTES-MWCNTs for RY2, zeta potential analysis was performed, and the results are displayed in Figure 4b. The pH_{IEP} (Isoelectric point of pH) of the MWCNTs increased from 5.7 to 10.1 after modification by APTES and PEI indicated that APETS and PEI successfully modified the MWCNTs. In addition, the surface of PEI/APTES-MWCNTs is positively charged when the solution pH is below 10.1 and negatively charged when the pH is above 10.1. On the other hand, the pK_a of primary, secondary, and tertiary amine groups are 4.5, 6.7, and 11.6, respectively [20]. Thus, at pH < pH_{IEP}, the primary and secondary amine groups on PEI/APTES-MWCNTs surface were protonated. The protonated primary (NH_3^+) and secondary (NH_2^+) amine groups readily bind to the negatively charged sulfonate groups ($-SO_3^{2-}$) of RY2 via electrostatic interaction [21]. On the contrary, the gradual deprotonation of protonated amine groups with the increase of pH reduced RY2 uptake [22]. When pH > pH_{IEP}, the surface of PEI/APTES-MWCNTs was entirely deprotonated, but the uptake of RY2 was still evident. In this case, the adsorption of RY2 on PEI/APTES-MWCNTs was mainly achieved by π–π stacking, hydrogen bonding, and van der Waals forces [15,23]. Since the maximum dye uptake was reached at pH 2, it was chosen for the subsequent studies.

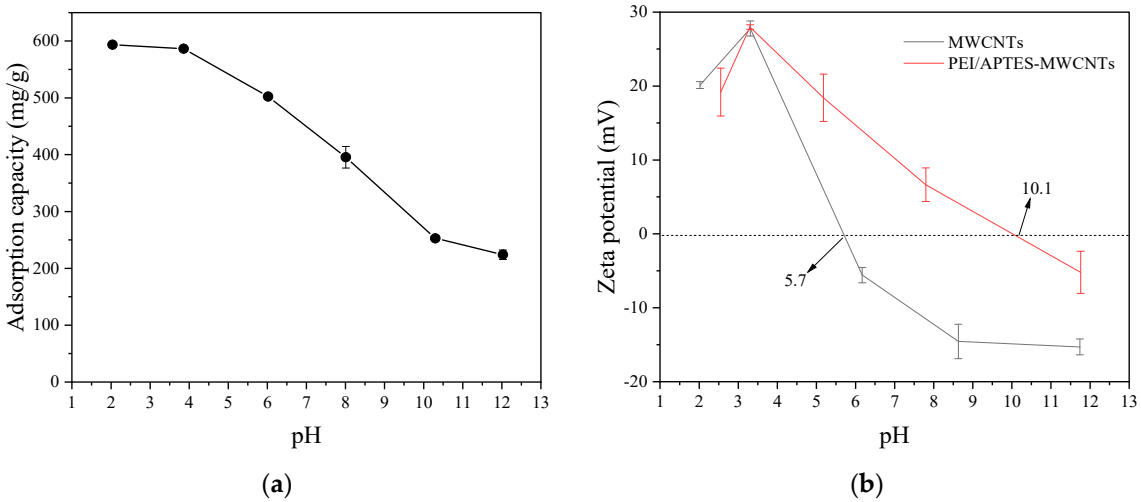

Figure 4. (a) Effect of pH on RY2 adsorption on PEI/APTES-MWCNTs and (b) zeta-potential of MWCNTs and PEI/APTES-MWCNTs at different pHs.

2.4. Adsorption Studies

Adsorption time, initial solute concentration, and solution temperature are leading factors that influence the adsorption performance of adsorbents. The effect of contact time, initial RY2

Preprints (www.preprints.org) | NOT PEER-REVIEWED | Posted: 9 January 2023 doi:10.20944/preprints202301.0154.v1

concentration, and temperature on RY2 adsorption onto PEI/APTES-MWCNTs were investigated, and the results are shown in Figure 5. Figure 5a displays the effect of contact time on the adsorption of RY2 onto PEI/APTES-MWCNTs at different initial concentrations. The time required to reach adsorption equilibrium was very short at low concentrations and pretty long at high concentrations. The time required for adsorption equilibrium was about 10, 15, and 180 min at initial concentrations of 50, 100, and 200 mg/L, respectively. It is worth noting that despite the relatively long time required to reach adsorption equilibrium at high concentrations (200 mg/L), 80% of its maximum adsorption capacity was attained within 30 min, which is of great interest in practical applications. Figure 5b demonstrates the influence of the initial RY2 concentration on its adsorption on PEI/APTES-MWCNTs, together with the influence of solution temperature evaluated by varying the temperature from 15 to 35 °C. It can be noticed that the slope of the curve is very steep at the initial stage, indicating that the removal of dyestuff at low concentrations was very high. The experimental results revealed that the removal rate of dyes in the initial concentration range of 30-200 mg/L was more than 95%. Moreover, as the temperature increased, the maximum adsorption capacity rose, indicating that the adsorption process was endothermic. For further understanding of the adsorption performance, kinetics, isotherm, and thermodynamic models were used to analyze the experimental data.

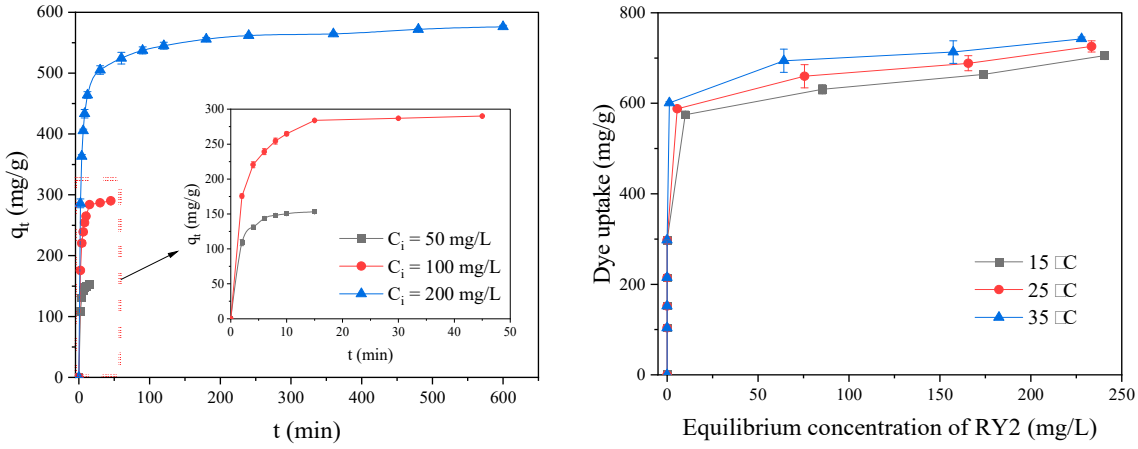

Figure 5. (a) Adsorption kinetics of RY2 on PEI/APTES-MWCNTs at 50–200 mg/L initial concentrations; (b) adsorption isotherm of RY2 on PEI/APTES-MWCNTs at different temperatures (15–35 °C).

2.4.1. Adsorption Kinetics

The adsorption rates, possible adsorption mechanisms, and potential rate-controlling steps of RY2 adsorption on PEI/APTES-MWCNTs were studied using pseudo-first-order (PFO), pseudo-second-order (PSO), and intraparticle diffusion (IPD) models. The linearized equation of the PFO [24], PSO [15], and IPD [25] models are as follows:

PFO model: $$\ln(q_e - q_t) = \ln q_e - k_1 t \quad (1)$$

PSO model: $$\frac{t}{q_t} = \frac{1}{k_2 q_e^2} + \frac{t}{q_e} \quad (2)$$

IPD model: $$q_t = k_i t^{0.5} + C \quad (3)$$

where q_t and q_e (mg/g) are the dye uptake at time t and equilibrium, respectively; k_1 (min^{-1}), k_2 (g/(mg·min)), and k_i (mg/(g·min$^{0.5}$)) are the rate constants of PFO, PSO, and IPD models, separately; C (mg/g) is the intercept which indicates the boundary layer thickness.

The curves fitted by the PFO and PSO models are displayed in Figure 6a–c, and the corresponding parameters are listed in Table 2. The value of the PSO model's correlation coefficient (*Adj.* R^2) was higher than that of the PFO model. Besides, the dye uptake at adsorption equilibrium

Preprints (www.preprints.org) | NOT PEER-REVIEWED | Posted: 9 January 2023 doi:10.20944/preprints202301.0154.v1

calculated by the PSO model was closer to that of the experimental data ($q_{e,exp}$). These facts suggested that the PSO model was more suitable to explain the kinetic process of RY2 adsorption on PEI/APTES-MWCNTs, and chemisorption dominated the adsorption process [21,26]. The rate constant (k_2) value decreased with increasing initial concentration of RY2, revealing that it was a concentration-dependent adsorption process [27]. The reason was that the total number of binding sites on the adsorbent surface was limited. As the dye concentration increased, excessive dye molecules competed for the limited adsorption sites, reducing the adsorption rate constant [28].

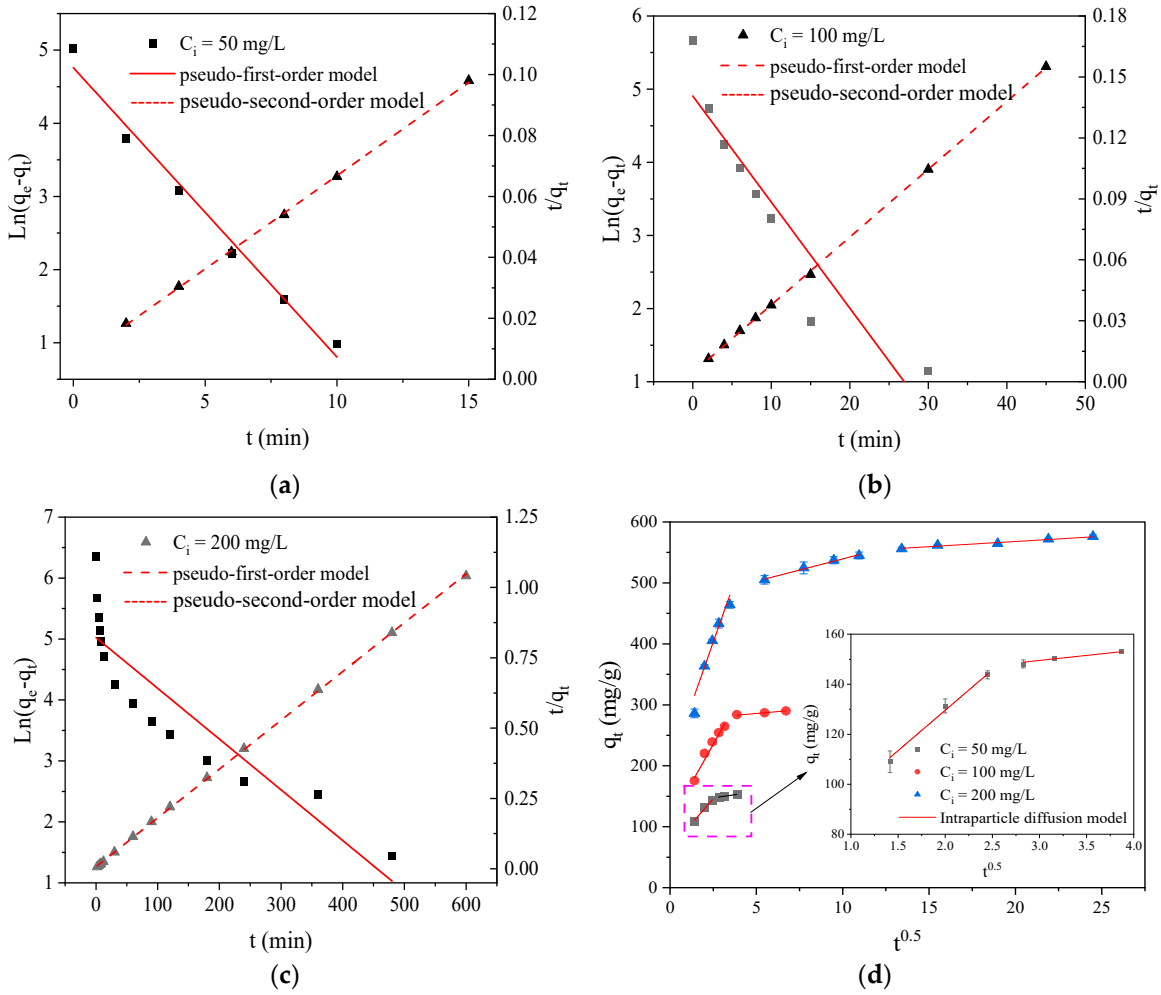

Figure 6. Pseudo-first/second-order modeling of RY2 adsorption on PEI/APTES-MWCNTs at an initial concentration of (a) 50, (b) 100, and (c) 200 mg/L, respectively; (d) intraparticle diffusion modeling of RY2 adsorption on PEI/APTES-MWCNTs.

The fitted curves of the IPD model and related parameters are depicted in Figure 6d and Table 2, respectively. The entire adsorption process mainly covers three sequences: (I) external surface diffusion, (II) intraparticle diffusion, and (III) adsorption equilibrium, according to the IPD model [29]. All the curves did not pass through the origin, indicating that the adsorption process was influenced by multiple rate-limiting stages [30]. At the initial RY2 concentrations of 50 and 100 mg/L, the fitted curves were split into two distinct regions, suggesting negligible intraparticle diffusion at low concentrations. On the contrary, the fitted curve was divided into three different regions at 200 mg/L initial concentration, demonstrating that the adsorption of RY2 on PEI/APTES-MWCNTs was controlled by external surface diffusion followed by intraparticle diffusion until adsorption equilibrium was reached [21]. Overall, at low concentrations, RY2 adsorption was scarcely affected by intraparticle diffusion, whereas at high concentrations it dominanted the adsorption process. On

Preprints (www.preprints.org) | NOT PEER-REVIEWED | Posted: 9 January 2023 doi:10.20944/preprints202301.0154.v1

the other hand, intraparticle diffusion was not the only rate-controlling stage, regardless of the concentration of RY2.

Table 2. Parameters of **p**seudo-first-order (PFO), pseudo-second-order (PSO), and intraparticle diffusion (IPD) models.

Models	Parameters	Initial Concentration (mg/L)		
		50	100	200
	$q_{e,exp}$ (mg/g)	153.03	290.10	576.15
PFO	q_1 (mg/g)	116.68	135.06	152.11
	k_1 (min^{-1})	0.3955	0.1450	0.0083
	Adj. R^2	0.9804	0.8583	0.5054
PSO	q_2 (mg/g)	163.40	299.40	578.03
	k_2 (g/(mg·min))	0.0057	0.0024	0.0004
	Adj. R^2	0.9995	0.9998	0.9999
IPD_{1st}	k_{i1} ($mg/(g·min^{0.5})$)	32.269	50.753	80.348
	C_{i1} (mg/g)	65.06	108.30	201.75
	Adj. R^2	0.9822	0.9686	0.9239
IPD_{2st}	k_{i2} ($mg/(g·min^{0.5})$)	4.028	2.478	7.330
	C_{i2} (mg/g)	137.43	273.47	466.17
	Adj. R^2	0.9781	0.9915	0.9852
IPD_{3st}	k_{i3} ($mg/(g·min^{0.5})$)			1.700
	C_{i3} (mg/g)	—	—	534.05
	Adj. R^2			0.9368

2.4.2. Adsorption Isotherms

To investigate whether adsorption occurs on homogeneous for heterogeneous surfaces, the Langmuir and Freundlich isotherm models were used to describe the experimental data. The linear equation of the Langmuir and Freundlich models are given below [15]:

Langmuir model: $$\frac{C_e}{q_e} = \frac{1}{K_L q_m} + \frac{C_e}{q_m} \quad (4)$$

Freundlich model: $$\ln q_e = \ln K_F + \frac{1}{n} \ln C_e \quad (5)$$

where q_e (mg/g) represents the maximum monolayer dye uptake, C_e (mg/L) and q_e (mg/g) are the concentration and adsorption capacity of RY2 at equilibrium; K_L (L/mg) and K_F ((mg/g)(L/mg)$^{1/n}$) are the Langmuir and Freundlich constants; n indicates the heterogeneity. The values of K_L and q_m were the slope and intercept of the curve plotted by C_e/q_e versus C_e, while the values of K_F and $1/n$ were calculated by the plot of $\ln q_e$ versus $\ln C_e$. To determine the favorability of adsorption, the separation factor (R_L) was also calculated using the following equation [26]:

$$R_L = \frac{1}{1 + K_L C_i} \quad (6)$$

where K_L (L/mg) is the Langmuir constant, and C_i (mg/L) is the initial RY2 concentration. The R_L values indicate whether the adsorption process is irreversible ($R_L = 0$), favorable ($0 < R_L < 1$), linear ($R_L = 1$), or unfavorable ($R_L > 1$).

The adsorption isotherm data fitted by the Langmuir and Freundlich models are shown in Figure 7, and the corresponding parameters are present in Table 3. The higher value of the correlation coefficient (*Adj.* R^2) of the Langmuir model revealed that it was more applicable to describe the isothermal sorption behavior. The experimental maximum adsorption capacities were close to the theoretical results calculated by the Langmuir model, further supporting its ability to interpret the

Preprints (www.preprints.org) | NOT PEER-REVIEWED | Posted: 9 January 2023 doi:10.20944/preprints202301.0154.v1

isothermal data. Therefore, the adsorption of RY2 on PEI/APTES-MWCNTs could attribute to monolayer adsorption on the homogeneous surface [31]. The Langmuir constant increased with temperature, indicating that the adsorption affinity of the adsorbent for RY2 was higher at high temperatures. The value of the separation factor was between 0 and 1, which was closer to 0, indicating that the adsorption of RY2 on PEI/APTES-MWCNTs was highly favorable. The theoretical maximum dye uptake was 689.66, 714.29, and 735.30 mg/g at 15, 25, and 35 °C, respectively, which were higher than most of the functionalized MWCNTs reported to date (Table 4). The maximum adsorption increased with temperature, indicating the adsorption process was endothermic. Thermodynamic analysis was performed to illustrate further the effect of temperature on the adsorption of RY2 by PEI/APTES-MWCNTs.

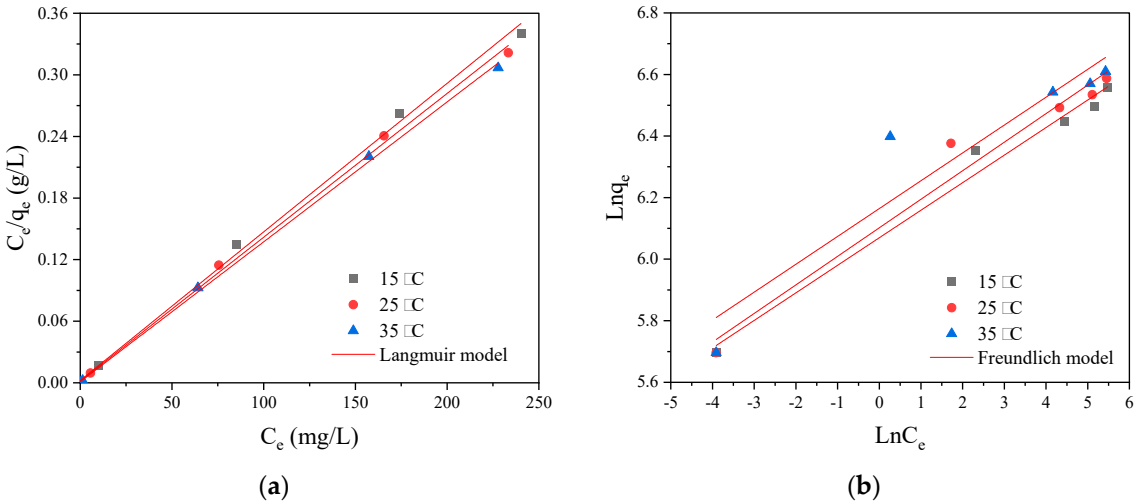

Figure 7. (a) Langmuir and (b) Freundlich modeling of RY2 adsorption on PEI/APTES-MWCNTs at 15, 25, and 35 °C.

Table 3. Langmuir and Freundlich parameters of RY2 adsorption on PEI/APTES-MWCNTs.

T (°C)	q_{exp} (mg/g)	Langmuir Model				Freundlich Model		
		q_{max} (mg/g)	K_L (L/mg)	R_L	*Adj.* R^2	K_F (mg/g)(L/mg)$^{1/n}$	*n*	*Adj.* R^2
15	705.10	689.66	0.6444	0.0001-0.0008	0.9977	432.49	11.17	0.9776
25	725.84	714.29	0.8333		0.9984	446.71	10.79	0.9570
35	742.43	735.30	1.3892		0.9992	475.49	11.05	0.8580

Table 4. Comparison of the adsorption capacities of functionalized MWCNTs for anionic dyes.

Adsorbent	Dye	q_m (mg/g)	T (°C)	pH	Ref.
PEI/APTES-MWCNTs	Reactive Yellow 2	689.66	15	2	This work
		714.29	25	2	
		735.29	35	2	
MWCNTs/Gly/β-CD	Acid Blue 113	172.41	25	7	[32]
	Methyl Orange	96.15	25	5	
	Disperse Red 1	500	25	7	
MWCNTs-NH_2	Acid Black 1	666	25	2	[33]
	Acid Black 25	714	25	2	
NH_2-MWCNTs	Methyl Orange	185.53	25	2	[34]
$MnFe_2O_4$/MWCNTs	Direct Red 16	607.79	55	2	[35]
MWCNTs-UiO-66	Methyl Red	105.26	25	3.61	[36]
MWCNTs/Fe_3O_4@(PDA + PEI)	Methyl Orange	935	25	7	[10]
	Congo Red	1006	25	7	

Preprints (www.preprints.org) | NOT PEER-REVIEWED | Posted: 9 January 2023 doi:10.20944/preprints202301.0154.v1

2.4.3. Thermodynamic Analysis

Temperature is a critical factor in the adsorption process. The effect of temperature on the adsorption of RY2 by PEI/APTES-MWCNTs is shown in Figure 5b. Thermodynamic parameters were calculated to determine the spontaneity of the adsorption activity, energy changes, and the degree of chaos. The standard Gibbs free energy ($\Delta G°$, kJ/mol), standard enthalpy ($\Delta H°$, kJ/mol), and standard enthalpy ($\Delta S°$, J/mol·K) were derived using the following equations [37]:

$$\Delta G° = -RT \ln K_e \tag{7}$$

$$\Delta G° = \Delta H° - T\Delta S° \tag{8}$$

$$\ln K_e = -\frac{\Delta H°}{RT} + \frac{\Delta S°}{R} \tag{9}$$

$$K_e = \frac{1000 K_L M C°}{\gamma} \tag{10}$$

where R stands for the universal gas constant (8.314 J/mol·K), T is the experimental temperature (K), K_e is a dimensionless parameter that denotes the thermodynamic equilibrium constant, K_L is the Langmuir constant (L/mg), M and $C°$ are the dye molecular weight (g/mol) and the standard dye concentration (mol/L), respectively, and γ, a dimensionless parameter, is the activity coefficient of RY2.

The plot of lnK_e versus $1/T$ determined the parameters as displayed in Table 5. The $\Delta G°$ values were negative, revealing that the adsorption of RY2 on PEI/APTES-MWCNTs was spontaneous in the temperature range of 15 to 35 °C. In contrast, the positive value of $\Delta H°$ suggested that the adsorption process was endothermic [38]. The significant and positive value of $\Delta S°$ indicates that the adsorption of RY2 on PEI/APTES-MWCNTs was an entropy-increasing process and an increase in randomness on the solid-liquid interface during the adsorption process [39]. Overall, the adsorption of RY2 onto PEI/APTES-MWCNTs was favorable at higher temperatures.

Table 5. Thermodynamic parameters of RY2 adsorption on PEI/APTES-MWCNTs.

T (°C)	K_e	ΔG (kJ/mol)	$\Delta H°$ (kJ/mol)	$\Delta S°$ (J/mol·K)	*Adj.* R^2
15	5.36×10^5	-31.58			
25	6.92×10^5	-33.32	28.21	207.27	0.9147
35	11.54×10^5	-35.75			

2.5. Effect of Ionic Strength

Industrial dye wastewater usually contains various ionic salts, typically NaCl [40]. Therefore, NaCl was selected to study the effect of interfering anions and cations on the adsorption of RY2 by PEI/APTES-MWCNTs. The experiment was performed by mixing 30 mL of 200 mg/L RY2 solutions (pH = 2) with 10 mg adsorbent under 25 °C for 24 h. The NaCl concentrations ranged from 0 to 0.1 mol/L; the results are demonstrated in Figure 8a. With the NaCl concentration increased from 0 to 0.1 mol/L, the adsorption capacity of PEI/APTES-MWCNTs for RY2 only decreased by less than 10%. This phenomenon indicated that cations and anions have little effect on the adsorption of reactive dye molecules on PEI/APTES-MWCNTs.

Preprints (www.preprints.org) | NOT PEER-REVIEWED | Posted: 9 January 2023 doi:10.20944/preprints202301.0154.v1

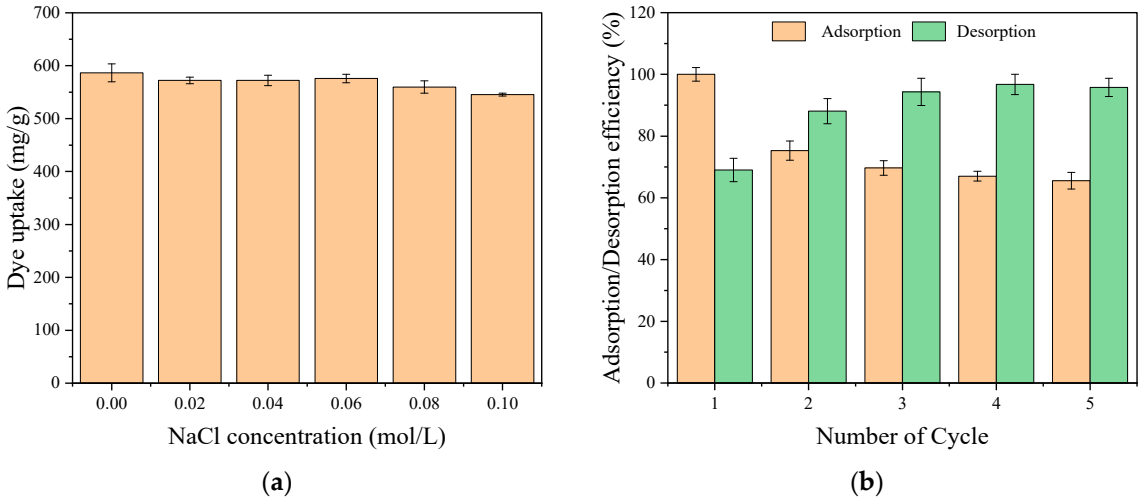

Figure 8. (a) Effect of ionic strength on RY2 adsorption by PEI/APTES-MWCNTs; (b) Adsorption/desorption efficiencies of PEI/APTES-MWCNTs for RY2 removal.

2.6. Reusability Studies

Reusability is an appealing quality of promising adsorbents, as it can reduce investment. The reusability of the PEI/APTES-MWCNTs was verified by conducting the adsorption/desorption cycle five times, and the results are displayed in Figure 8b. The adsorption efficiency remarkably decreased from 100.0 to 75.3% after the first adsorption/desorption cycle. Hereafter, it decreased slightly to 65.6% after five adsorption/desorption cycles. On the contrary, the desorption efficiency increased notably from 69.0% to 94.3% from the first to the third cycles. Then, it remained stable at 96.0 ± 1.0% for the following cycles. Although the adsorption capacity of the adsorbent was lost by about 25% after the first adsorption/desorption cycle, the loss was less in the subsequent cycles and even negligible after the third cycle, so the adsorbent can be considered to have a good potential for industrial applications.

3. Materials and Methods

3.1. Materials

MWCNTs (Diameter: 8-15 nm; Length: 5-20 μm; Grade: TMC-100-10; purity: > 90 wt%) were supplied by Nano Solution Co., Ltd. (Jeonju, Korea). Branched PEI (M_w: 70,000, 50% (w/v) aq. Soln.) was obtained from Habjung Moolsan Co., Ltd. (Seoul, Korea). APTES (99%) was purchased from Daejung Chemical & Metals Co., Ltd. (Siheung, Korea). Epichlorohydrin (ECH, ≥ 99%) and RY2 (Content: 60 ~ 70%) were purchased from Sigma-Aldrich Korea Ltd. (Yongin, Korea). All of the other chemicals used in this study were of analytical grade.

3.2. Preparation of PEI/APTES-MWCNTs

The preparation of PEI/APTES-MWCNTs consists of two steps: grafting APTES on MWCNTs surface and crosslinking of PEI with APTES-MWCNTs using ECH as crosslinker. The scheme of the preparation process is illustrated in Figure 9. Here are the details:

Step I: APTES-MWCNTs were prepared according to the method of Anton et al. (2020) [41] with slight modifications. Briefly, 1.5 g of MWCNTs were dispersed in 300 mL of 5% APTES solution (pH = 5, adjusted by CH_3COOH). The solution was homogenized at 13,500 rpm for 10 min using a WiseTis homogenizer (HG-15A, Witeg, Germany). The mixture was refluxed at 80 °C for 12 h with continuous stirring at 100 rpm. The resulting product (APTES-MWCNTs) was washed several times with distilled water until pH = 7 and collected by filtration through a 0.22 μm PVDF membrane. One-third of the product (approximately equivalent to 0.5 g MWCNTs) was then taken out, freeze-dried for 24 h, and set aside for further use, while the rest was used in the next step.

Preprints (www.preprints.org) | NOT PEER-REVIEWED | Posted: 9 January 2023 doi:10.20944/preprints202301.0154.v1

Step II: The APTES-MWCNTs prepared in the first step (approximately equivalent to 1.0 g MWCNTs) were mixed with 240 mL of 2% ECH solution and homogenized for 5 min. Then, 160 mL of 2.5 wt% PEI solution was added to this mixture and homogenized again for 10 min. The mixing solution was stirred continuously at 300 rpm for 12 h at room temperature (25 ± 1 °C). The final product (PEI/APTES-MWCNTs) was filtered and rinsed against distilled water several times until the filtrate was neutral. The PEI/APTES-MWCNTs were dried for 24 h using a freeze dryer and then stored in a desiccator for future experiments.

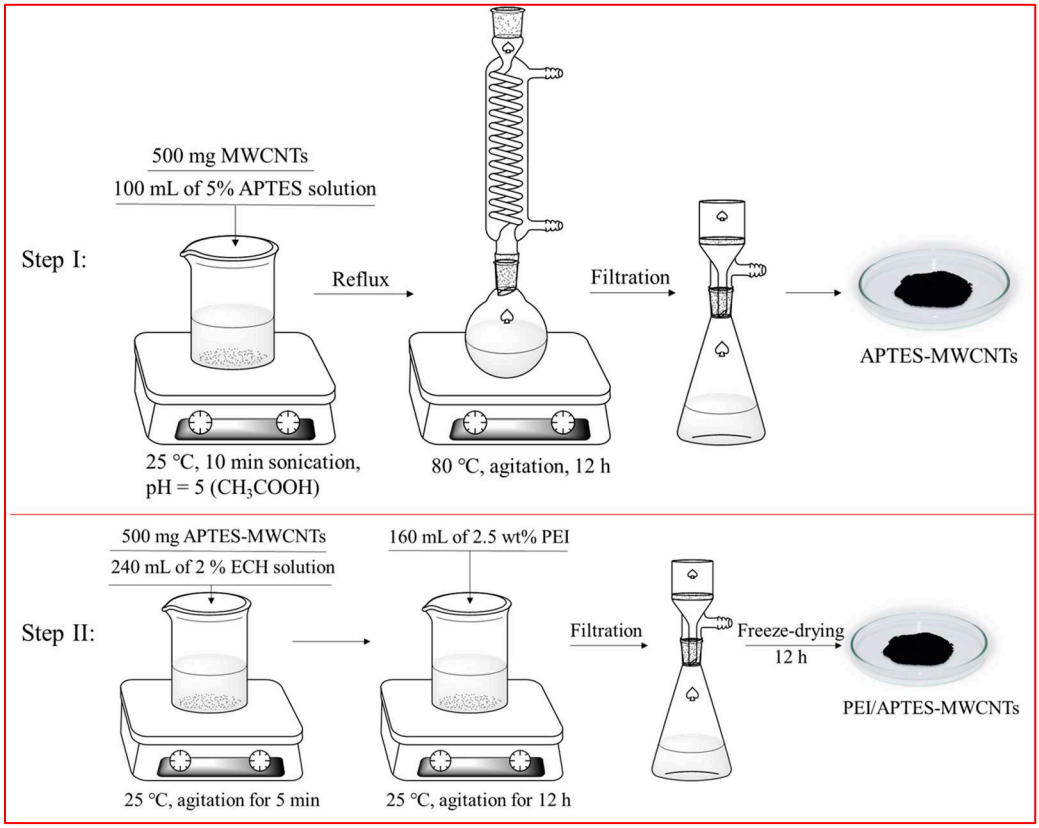

Figure 9. Scheme of the process of PEI/APTES-MWCNTs preparation.

3.3. Characterization of Samples

The surface morphologies of the materials were observed using FE-SEM (Apreo S, Thermo Fisher, USA). The elemental mapping was simultaneously recorded using an EDS (Ultim®MAX, ORFORD Instrument, UK). BET analysis was conducted using a specific surface area analyzer (3 Flex, Micromeritics, USA). The zeta-potentials of MWCNTs and PEI/APTES-MWCNTs were analyzed using a zeta-potential analyzer (ELSZ-2000, Otsuka, Japan).

3.4. Adsorption Experiments

The pH edge experiments were performed for 24 h using an initial dye concentration of 200 mg/L in the pH range of 2–12, and the pH was adjusted using 1 M NaOH or 1 M HCl. Adsorption kinetics experiments were conducted in 50, 100, and 200 mg/L initial dye concentrations at pH 2. Adsorption isotherm experiments were performed at initial dye concentrations ranging from 30 to 500 mg/L at pH 2 for 24 h. The effect of temperature on the adsorption of dyes by PEI/APTES-MWCNTs was also performed at 288, 298, and 308 K. The effect of ionic strength was evaluated by adding a certain amount of NaCl into 30 mL of 200 mg/L RY2 solutions, making the NaCl concentrations range from 0 to 0.1 mol/L. The dye concentrations before and after adsorption experiments were measured using a UV-Vis spectrophotometer (X-ma 3000 pc, Human, Korea). All adsorption experiments were conducted by mixing 10 mg of adsorbent with 30 mL of RY2 solution (pH = 2) in 50 mL falcon tubes. The tubes were placed in a multi-shaking incubator at 160 rpm and 25 ℃. Samples were prepared in

Preprints (www.preprints.org) | NOT PEER-REVIEWED | Posted: 9 January 2023 doi:10.20944/preprints202301.0154.v1

triplicate in all adsorption experiments. The dye uptake (q, mg/g) was calculated using the equation below:

$$q = \frac{C_i V_i - C_f V_f}{m} \quad (11)$$

where C_i and C_f are the initial and final dye concentrations (mg/L), respectively; V_i and V_f are the solution volume (mL) before and after adsorption experiments; m is the adsorbent weight (g).

3.5. Reusability Experiments

First, RY2-loaded adsorbent was prepared by mixing 10 mg of PEI/APTES-MECNTs with 30 mL of 200 mg/L RY2 solutions for 10 h. The dye-loaded adsorbent was rinsed with distilled water (pH = 2) two times and subjected to desorption. The dye-loaded adsorbent was mixed with 30 mL of alkaline acetone solution (prepared by mixing 0.2 M NaOH and acetone in the volume ratio of 1:1) in 50-mL falcon tubes and placed in a multi-shaking incubator at 25 °C and 160 rpm for 2 h. After centrifugation, the supernatant was used to measure the concentration of the desorbed dye. The desorbed adsorbent was washed three times with distilled water and then used in the next adsorption-desorption cycle. The regeneration experiments were performed five times in total. The adsorption and desorption efficiencies were calculated using Eqs. (12) and (13).

$$Adsorption\ efficiency\ (\%) = \frac{\text{Adsorbed dye amount in each cycle (mg)}}{\text{Original dye adsorption amount (mg)}} \times 100 \quad (12)$$

$$Desorption\ efficiency\ (\%) = \frac{\text{Desorbed dye amount in each cycle (mg)}}{\text{Adsorbed dye amount in each cycle (mg)}} \times 100 \quad (13)$$

4. Conclusions

In this study, we prepared amine-functionalized MWCNTs, namely PEI/APTES-MWCNTs, by a facile method. FE-SEM-EDS, BET, and zeta potential analysis proved that the material was successfully prepared. The adsorption performance of the PEI/APTES-MWCNTs for reactive dyes was evaluated using RY2 as a representative. One-point-check experiment results exhibited that the adsorption capacity of RY2 on PEI/APTES-MWCNTs was 2.8 times higher than that of MWCNTs. Kinetic studies showed that the PEI/APTES-MWCNTs is an effective adsorbent capable of rapidly eliminating reactive dyes from aqueous solutions over a wide range of initial concentrations. Specifically, at an initial concentration of 50-100 mg/L, more than 99% of the dye molecules could be separated from water in less than 15 min. When the initial concentration was increased to 200 mg/L, over 80% of the dye molecules could still be isolated from water within 30 min. Isotherm studies showed that the maximum dye uptake at 15, 25, and 35 °C was 689.66, 714.29, and 735.30 mg/g, separately. The PSO model better explained the kinetic adsorption process, and the Langmuir model was better suited to explain the adsorption isotherm process. Thermodynamic studies revealed that the adsorption process was spontaneous and endothermic. The effect of ionic strength indicated that the adsorbent has excellent resistance to ionic salt interference. The reusability study revealed that the adsorbent has good reusability. In conclusion, the PEI/APTES-MWCNTs are effective and reusable adsorbents for rapid and highly efficient adsorption of reactive dyes from aqueous solutions.

Author Contributions: Conceptualization, Zhuo Wang; Data curation, Zhuo Wang; Formal analysis, Zhuo Wang; Funding acquisition, Sung Wook Won; Investigation, Zhuo Wang; Methodology, Zhuo Wang; Project administration, Sung Wook Won; Resources, Zhuo Wang; Supervision, Sung Wook Won; Validation, Zhuo Wang; Visualization, Zhuo Wang; Writing – original draft, Zhuo Wang; Writing – review & editing, Sung Wook Won. All authors have read and agreed to the published version of the manuscript.

Funding: This research was funded by the National Research Foundation of Korea (NRF) grant funded by the Ministry of Science and ICT (South Korea), grant number 2020R1F1A1065937.

Institutional Review Board Statement: Not applicable.

Informed Consent Statement: Not applicable.

Data Availability Statement: All data generated in this study is presented in the current manuscript. Data is available upon request from the corresponding author.

Conflicts of Interest: The authors declare no conflict of interest.

References

1. Boretti, A.; Rosa, L., Reassessing the projections of the World Water Development Report. *npj Clean Water* **2019,** 2, (1), 15.
2. Angelakis, A. N.; Valipour, M.; Ahmed, A. T.; Tzanakakis, V.; Paranychianakis, N. V.; Krasilnikoff, J.; Drusiani, R.; Mays, L.; El Gohary, F.; Koutsoyiannis, D.; Khan, S.; Giacco, L. J. D., Water Conflicts: From Ancient to Modern Times and in the Future. *Sustainability* **2021,** 13, (8), 4237.
3. Huang, Z.; Liu, X.; Sun, S.; Tang, Y.; Yuan, X.; Tang, Q., Global assessment of future sectoral water scarcity under adaptive inner-basin water allocation measures. *Science of The Total Environment* **2021,** 783, 146973.
4. Khan, A. A.; Gul, J.; Naqvi, S. R.; Ali, I.; Farooq, W.; Liaqat, R.; AlMohamadi, H.; Štěpanec, L.; Juchelková, D., Recent progress in microalgae-derived biochar for the treatment of textile industry wastewater. *Chemosphere* **2022,** 306, 135565.
5. Khatri, A.; Peerzada, M. H.; Mohsin, M.; White, M., A review on developments in dyeing cotton fabrics with reactive dyes for reducing effluent pollution. *Journal of Cleaner Production* **2015,** 87, 50-57.
6. Wang, L.; Tao, Y.; Wang, J.; Tian, M.; Liu, S.; Quan, T.; Yang, L.; Wang, D.; Li, X.; Gao, D., A novel hydroxyl-riched covalent organic framework as an advanced adsorbent for the adsorption of anionic azo dyes. *Analytica Chimica Acta* **2022,** 1227, 340329.
7. Azari, A.; Nabizadeh, R.; Nasseri, S.; Mahvi, A. H.; Mesdaghinia, A. R., Comprehensive systematic review and meta-analysis of dyes adsorption by carbon-based adsorbent materials: Classification and analysis of last decade studies. *Chemosphere* **2020,** 250, 126238.
8. Saxena, R.; Saxena, M.; Lochab, A., Recent Progress in Nanomaterials for Adsorptive Removal of Organic Contaminants from Wastewater. *ChemistrySelect* **2020,** 5, (1), 335-353.
9. Saravanan, A.; Kumar, P. S.; Hemavathy, R. V.; Jeevanantham, S.; Jawahar, M. J.; Neshaanthini, J. P.; Saravanan, R., A review on synthesis methods and recent applications of nanomaterial in wastewater treatment: Challenges and future perspectives. *Chemosphere* **2022,** 307, 135713.
10. Zhao, S.; Zhan, Y.; Wan, X.; He, S.; Yang, X.; Hu, J.; Zhang, G., Selective and efficient adsorption of anionic dyes by core/shell magnetic MWCNTs nano-hybrid constructed through facial polydopamine tailored graft polymerization: Insight of adsorption mechanism, kinetic, isotherm and thermodynamic study. *Journal of Molecular Liquids* **2020,** 319, 114289.
11. Rajabi, M.; Mahanpoor, K.; Moradi, O., Removal of dye molecules from aqueous solution by carbon nanotubes and carbon nanotube functional groups: critical review. *RSC Advances* **2017,** 7, (74), 47083-47090.
12. Hadavifar, M.; Bahramifar, N.; Younesi, H.; Li, Q., Adsorption of mercury ions from synthetic and real wastewater aqueous solution by functionalized multi-walled carbon nanotube with both amino and thiolated groups. *Chemical Engineering Journal* **2014,** 237, 217-228.
13. Gao, L.; Zhang, Q.; Guo, J.; Li, H.; Wu, J.; Yang, X.; Sui, G., Effects of the amine/epoxy stoichiometry on the curing behavior and glass transition temperature of MWCNTs-NH_2/epoxy nanocomposites. *Thermochimica Acta* **2016,** 639, 98-107.
14. Chu, Y.; Tang, D.; Ke, Z.; Ma, J.; Li, R., Polyethylenimine-functionalized multiwalled carbon nanotube for the adsorption of hydrogen sulfide. *Journal of Applied Polymer Science* **2017,** 134, (16),44742.
15. Saleh, T. A.; Elsharif, A. M.; Bin-Dahman, O. A., Synthesis of amine functionalization carbon nanotube-low symmetry porphyrin derivatives conjugates toward dye and metal ions removal. *Journal of Molecular Liquids* **2021,** 340, 117024.
16. Thommes, M.; Kaneko, K.; Neimark, A. V.; Olivier, J. P.; Rodriguez-Reinoso, F.; Rouquerol, J.; Sing, K. S., Physisorption of gases, with special reference to the evaluation of surface area and pore size distribution (IUPAC Technical Report). *Pure and applied chemistry* **2015,** 87, (9-10), 1051-1069.
17. Wang, Z.; Kang, S. B.; Yun, H. J.; Won, S. W., Polyethylenimine-crosslinked chitin biosorbent for efficient recovery of Pd(II) from acidic solution: Characterization and adsorption mechanism. *Carbohydrate Polymer Technologies and Applications* **2021,** 2, 100091.
18. Xu, T.; Qu, R.; Zhang, Y.; Sun, C.; Wang, Y.; Kong, X.; Geng, X.; Ji, C., Preparation of bifunctional polysilsesquioxane/carbon nanotube magnetic composites and their adsorption properties for Au (III). *Chemical Engineering Journal* **2021,** 410, 128225.
19. Khakpour, R.; Tahermansouri, H., Synthesis, characterization and study of sorption parameters of multi-walled carbon nanotubes/chitosan nanocomposite for the removal of picric acid from aqueous solutions. *International Journal of Biological Macromolecules* **2018,** 109, 598-610.
20. Hamza, M. F.; Lu, S.; Salih, K. A. M.; Mira, H.; Dhmees, A. S.; Fujita, T.; Wei, Y.; Vincent, T.; Guibal, E., As(V) sorption from aqueous solutions using quaternized algal/polyethyleneimine composite beads. *Science of The Total Environment* **2020,** 719, 137396.

21. Wang, Z.; Bin Kang, S.; Won, S. W., Polyethylenimine-aminated polyvinyl chloride fiber for adsorption of reactive dyes from single and binary component systems: Adsorption kinetics and isotherm studies. *Colloids and Surfaces A: Physicochemical and Engineering Aspects* **2022,** 647, 128983.
22. Mahmoud, M. E.; Abdelfattah, A. M.; Tharwat, R. M.; Nabil, G. M., Adsorption of negatively charged food tartrazine and sunset yellow dyes onto positively charged triethylenetetramine biochar: Optimization, kinetics and thermodynamic study. *Journal of Molecular Liquids* **2020,** 318, 114297.
23. Gao, M.; Xu, D.; Gao, Y.; Chen, G.; Zhai, R.; Huang, X.; Xu, X.; Wang, J.; Yang, X.; Liu, G., Mussel-inspired triple bionic adsorbent: Facile preparation of layered double hydroxide@polydopamine@metal-polyphenol networks and their selective adsorption of dyes in single and binary systems. *Journal of Hazardous Materials* **2021,** 420, 126609.
24. Simonin, J.-P., On the comparison of pseudo-first order and pseudo-second order rate laws in the modeling of adsorption kinetics. *Chemical Engineering Journal* **2016,** 300, 254-263.
25. Alves, D. C. S.; Gonçalves, J. O.; Coseglio, B. B.; Burgo, T. A. L.; Dotto, G. L.; Pinto, L. A. A.; Cadaval, T. R. S., Adsorption of phenol onto chitosan hydrogel scaffold modified with carbon nanotubes. *Journal of Environmental Chemical Engineering* **2019,** 7, (6), 103460.
26. Ashrafi, S. D.; Safari, G. H.; Sharafi, K.; Kamani, H.; Jaafari, J., Adsorption of 4-Nitrophenol on calcium alginate-multiwall carbon nanotube beads: Modeling, kinetics, equilibriums and reusability studies. *International Journal of Biological Macromolecules* **2021,** 185, 66-76.
27. Marrakchi, F.; Hameed, B. H.; Bouaziz, M., Mesoporous and high-surface-area activated carbon from defatted olive cake by-products of olive mills for the adsorption kinetics and isotherm of methylene blue and acid blue 29. *Journal of Environmental Chemical Engineering* **2020,** 8, (5), 104199.
28. Ofomaja, A. E.; Naidoo, E. B.; Modise, S. J., Kinetic and Pseudo-Second-Order Modeling of Lead Biosorption onto Pine Cone Powder. *Industrial & Engineering Chemistry Research* **2010,** 49, (6), 2562-2572.
29. Liu, B.; Chen, T.; Wang, B.; Zhou, S.; Zhang, Z.; Li, Y.; Pan, X.; Wang, N., Enhanced removal of Cd^{2+} from water by AHP-pretreated biochar: Adsorption performance and mechanism. *Journal of Hazardous Materials* **2022,** 438, 129467.
30. Zhang, L.; Cheng, H.; Pan, D.; Wu, Y.; Ji, R.; Li, W.; Jiang, X.; Han, J., One-pot pyrolysis of a typical invasive plant into nitrogen-doped biochars for efficient sorption of phthalate esters from aqueous solution. *Chemosphere* **2021,** 280, 130712.
31. Birtane, H.; Urucu, O. A.; Yıldız, N.; Çiğil, A. B.; Kahraman, M. V., Statistical optimization and selective uptake of Au(III) from aqueous solution using carbon nanotube-cellulose based adsorbent. *Materials Today Communications* **2022,** 30, 103114.
32. Mohammadi, A.; Veisi, P., High adsorption performance of β-cyclodextrin-functionalized multi-walled carbon nanotubes for the removal of organic dyes from water and industrial wastewater. *Journal of Environmental Chemical Engineering* **2018,** 6, (4), 4634-4643.
33. Maleki, A.; Hamesadeghi, U.; Daraei, H.; Hayati, B.; Najafi, F.; McKay, G.; Rezaee, R., Amine functionalized multi-walled carbon nanotubes: Single and binary systems for high capacity dye removal. *Chemical Engineering Journal* **2017,** 313, 826-835.
34. Liu, Y.; Cui, G.; Luo, C.; Zhang, L.; Guo, Y.; Yan, S., Synthesis, characterization and application of amino-functionalized multi-walled carbon nanotubes for effective fast removal of methyl orange from aqueous solution. *RSC Advances* **2014,** 4, (98), 55162-55172.
35. Kafshgari, L. A.; Ghorbani, M.; Azizi, A., Fabrication and investigation of $MnFe_2O_4$/MWCNTs nanocomposite by hydrothermal technique and adsorption of cationic and anionic dyes. *Applied Surface Science* **2017,** 419, 70-83.
36. Athari, M.; Fattahi, M.; Khosravi-Nikou, M.; Hajhariri, A., Adsorption of different anionic and cationic dyes by hybrid nanocomposites of carbon nanotube and graphene materials over UiO-66. *Scientific Reports* **2022,** 12, (1), 20415.
37. Lima, E. C.; Hosseini-Bandegharaei, A.; Moreno-Piraján, J. C.; Anastopoulos, I., A critical review of the estimation of the thermodynamic parameters on adsorption equilibria. Wrong use of equilibrium constant in the Van't Hoof equation for calculation of thermodynamic parameters of adsorption. *Journal of Molecular Liquids* **2019,** 273, 425-434.
38. Haq, F.; Farid, A.; Ullah, N.; Kiran, M.; Khan, R. U.; Aziz, T.; Mehmood, S.; Haroon, M.; Mubashir, M.; Bokhari, A.; Chuah, L. F.; Show, P. L., A study on the uptake of methylene blue by biodegradable and eco-friendly carboxylated starch grafted polyvinyl pyrrolidone. *Environmental Research* **2022,** 215, 114241.
39. Alaguprathana, M.; Poonkothai, M.; Ameen, F.; Ahmad Bhat, S.; Mythili, R.; Sudhakar, C., Sodium hydroxide pre-treated Aspergillus flavus biomass for the removal of reactive black 5 and its toxicity evaluation. *Environmental Research* **2022,** 214, 113859.
40. Liu, Z.; Qiang, R.; Lin, L.; Deng, X.; Yang, X.; Zhao, K.; Yang, J.; Li, X.; Ma, W.; Xu, M., Thermally modified polyimide/SiO_2 nanofiltration membrane with high permeance and selectivity for efficient dye/salt separation. *Journal of Membrane Science* **2022,** 658, 120747.

41. Mostovoy, A.; Yakovlev, A.; Tseluikin, V.; Lopukhova, M., Epoxy Nanocomposites Reinforced with Functionalized Carbon Nanotubes. *Polymers (Basel)* **2020,** 12, (8), 1816.